Low temperature autoignition of diesel fuel under dual operation with hydrogen and hydrogen-carriers

Hernández, Juan J.; Cova Bonillo, Alexis; Wu, Han; Barba, Javier; Rodríguez-Fernández, José

DOI:
10.1016/j.enconman.2022.115516

Energy Conversion and Management 258 (2022) 115516

Contents lists available at ScienceDirect

Energy Conversion and Management

journal homepage: www.elsevier.com/locate/enconman

Low temperature autoignition of diesel fuel under dual operation with hydrogen and hydrogen-carriers

Juan J. Hernández [a,*], Alexis Cova-Bonillo [a], Han Wu [b], Javier Barba [a], José Rodríguez-Fernández [a]

[a] University of Castilla-La Mancha, Escuela Técnica Superior de Ingeniería Industrial, Edificio Politécnico, Avda. Camilo José Cela s/n, 13071 Ciudad Real, Spain
[b] School of Mechanical Engineering, Beijing Institute of Technology (BIT), Beijing 100081, China

ARTICLE INFO

Keywords:
Autoignition
Dual-fuel combustion
Hydrogen-carriers

ABSTRACT

While electrification of light duty vehicles is becoming a real solution to abate local pollutant as well as greenhouse gases emission, heavy duty applications (such as long distance, freight and maritime transport) will keep requiring fuel-based propulsion systems. In these sectors, dominated by compression ignition engines, research on alternative biofuels and new combustion modes is still highly necessary. Dual-fuel combustion appears as a very promising concept to replace conventional diesel fuel by sustainable ones. Among the latter, hydrogen-derived fuels (the so-called electrofuels or e-fuels) are maybe the most interesting. This work addresses the effect of partial substitution of diesel fuel by hydrogen and hydrogen-carriers (ammonia and methane) on the autoignition process under low temperature conditions. Tests were carried out in a constant volume combustion chamber at different temperatures (535, 600 and 650 °C) and pressures (11, 16 and 21 bar). While the cool flames timing and intensity was only slightly affected by the low reactivity fuel energy content, the main ignition was delayed, this effect being much more noticeable for ammonia, followed by hydrogen and finally methane. Kinetic simulations showed a clear competition for active radicals between both fuels (diesel and low reactivity fuel). The combustion duration also increased with the hydrogen or hydrogen-carrier content, which greatly points to the need of modifications in the injection strategy of compression ignition engines operating under dual mode. A correlation was proposed for estimating the autoignition delay time for dual-fuel lean combustion at low temperature.

1. Introduction

Electrification of light-duty vehicles is emerging as the most cost-effective technology to reduce local pollutant emissions and to promote sustainable mobility [1]. However, applications for medium and heavy-duty are still a significant challenge since the energy density of batteries and fuel cells (together with the very high cost of the latter) does not allow for their widespread and practical use [2]. These applications include maritime, freight and long-distance road transport, as well as stationary production of electricity/heat (electrical generators and cogeneration plants). As these sectors are mainly dominated by compression ignition (CI) engines, research on new combustion modes, sustainable fuels and aftertreatment technologies for limiting tailpipe pollution as well as for increasing the efficiency (and thus reducing CO_2 emissions) is still highly needed [2].

Dual-fuel CI combustion has appeared in the last years as a very promising concept for either decreasing pollutant emissions (mainly nitrogen oxides, NOx, and particulate matter, PM), or for replacing the fossil diesel fuel by an alternative one, the latter with renewable origin and/or with a low carbon content. This combustion mode is based on the simultaneous use of two fuels, the conventional one being usually fed into the combustion chamber (direct injection, DI) and the second fuel being introduced either through port fuel (PFI) [3] or direct injection [4] (the former being most common because it does not require significant engine structure modifications). Since the reactivity of the DI fuel uses to be higher than that of the PFI fuel, the former was identified in this work as HRF (high reactivity fuel) and the latter as LRF (low reactivity fuel) for clarification. This nomenclature matches that used for RCCI (Reactivity Controlled Compression Ignition) operation, although RCCI is a more specific dual-fuel combustion mode looking for high efficiencies and very low pollutant emissions by optimizing the injection strategy as well as the HRF/LRF ratio depending on the engine load (not necessarily

* Corresponding author.
E-mail address: JuanJose.Hernandez@uclm.es (J.J. Hernández).

https://doi.org/10.1016/j.enconman.2022.115516
Received 3 December 2021; Received in revised form 15 March 2022; Accepted 16 March 2022
Available online 22 March 2022

involving sustainable fuels). As described in recent review works, different studies on engine dual-fuel combustion have been reported in the literature, natural gas (mainly composed by methane, CH_4) [5] and hydrogen (H_2) [6] being the most widely tested fuels because of its lower or nil specific carbon dioxide (CO_2) emissions when compared to conventional liquid fuels. Works on ammonia (NH_3) [7], liquified petroleum gas (LPG) [8], methanol [9], syngas [10], biogas [6] and other compounds [11] have also been reported.

The worldwide hydrogen production represents approximately 7.7 EJ/year (about 51% of which is used for ammonia production [12]). According to the Hydrogen Council production [12], hydrogen demand will increase from 5 to 10%, with expectations of fulfil 18% of energy demand by 2050 and preventing 6 Gt of CO_2 emissions annually. Essentially, H_2 is the nil-carbon fuel par excellence, with zero direct CO_2 emissions. Life-cycle CO_2 depends on whether the production process is renewable or it comes from a fossil source (oil, coal, or natural gas) [13]. Water electrolysis provides an efficient, clean and proven alternative production technology [14], which can be integrated with renewable electricity from solar and wind power to establish the so-called *Power*-to-*X* (*PtX*) schemes [15]. Electrolysis produces about 4% of the H_2 world's production [16], the rest coming from non-renewable sources by techniques including coal gasification, methane-steam reforming [17], liquid fuels reforming and biochemical conversion [18]. Several interesting reviews have been published on green hydrogen production methods [17,19].

Ammonia is the second most manufactured chemical in the world (176 million tonnes [20]). Although it is very mostly used as fertilizer, it may be rapidly emerging as a potentially revolutionary source of clean energy. In fact, the possibility of an ammonia-based energy future is currently being discussed in literature [21,22]. Moreover, global ammonia production capacity is expected to rise from about 235 in 2019 to approximately 290 million metric tons in 2030 [23]. Although there are several production processes, the most important is the Haber-Bosch (HB) thermo-catalytic synthesis, which dominates the market [24], and in a lesser extent other methods based on electrochemical synthesis. MacFarlane et al. [25] described the evolution of the ammonia production process through three types of technologies or generations, in which the third generation avoids the HB process. As hydrogen, ammonia does not emit direct CO_2. Due to its high energy density, NH_3 is an excellent H_2 carrier [26]. Among the advantages over H_2 is the long-term storage capacity, since it can be liquefied at pressures of 8–10 bar at room temperature, hydrogen requiring much higher values or cryogenic storage. Another key competitive advantage is that ammonia production, transportation, and distribution infrastructure is in place worldwide. Even though ammonia has also important safety concerns related to its toxic character and corrosive nature, it permits safer handling and distribution compared to hydrogen. Despite its toxicity, its odour can be detected even at very low concentration levels (<1 ppm). Because of the possible need of NOx removal devices, the use of ammonia seems to be more cost-effective for shipping applications, since no space restrictions are expected [7].

As for methane, it is the main component of natural gas (NG) and the most cost-effective electrofuel [27]. Its availability is probably the most widespread in the world, which is an important advantage. In addition, there are many renewable production techniques [28]. Although the production of methane from waste is a longstanding practice (biomethane or biogas) [29], the concept of synthetic natural gas (SNG) obtained from CO_2-captured and green-H_2 has recently emerged [30]. It is well known its direct use in vehicles based on spark ignition engines (natural gas for vehicles or NGV [28]). Under dual-fuel CI mode, as commented above, it has been used as the main diesel fuel substitute. This is due to the simplicity of the molecule, with no carbon–carbon bonds and a high H/C ratio. World natural gas production was about 3.9 trillion cubic meters in 2020 [31]. Among fossil fuels, this is the only one whose production is expected to increase by 2035 [32].

The three above mentioned fuels (H_2, NH_3 and CH_4) were tested in this work as LRFs. The existing literature on dual-fuel combustion is broad, but not much specifically focuses on the autoignition process (the objective of the present work), which greatly affects the engine efficiency and the pollutant emissions of CI engines. Although an exhaustive review is beyond the scope of this paper, some relevant and general insights are addressed below.

In a previous work, the authors analysed the autoignition behaviour of diesel and biodiesel fuels under a hydrogen-rich atmosphere in a constant volume combustion chamber. 10% and 20% of the energy of the liquid fuels was replaced by H_2 at different temperatures and equivalence ratios. They found that hydrogen delays autoignition and reduces the combustion rate of the diesel fuel because of a reduction of the OH radical pool [33]. Other studies carried out in engines [34,35] and under very different conditions also showed a delay on the combustion onset when hydrogen replaced diesel fuel. The review by Chintala and Subramanian [36] reported that both the effect on the autoignition time as well as on the in-cylinder pressure peak depends not only on the amount of hydrogen but also on the engine load. They reported that this fluctuating trend is due to several and sometimes opposing H_2-derived phenomena, which include a higher concentration of free radicals from H_2 pre-reactions, a lower in-cylinder oxygen content because of the air displacement and a higher specific heat of the compressed charge.

Feng et al [37] studied the autoignition properties of NH_3/diesel binary blends, at various NH_3 blending ratios (10%, 30% and 50% by energy) in a rapid compression machine (RCM). Ignition delay times were measured spanning a temperature range of 670–910 K, pressures of 10–20 bar, and equivalence ratios of 0.5–1.5. The authors concluded that NH_3 addition has a significant nonlinear effect on the low-temperature ignition of the blends as result of the competition for •OH radicals between both fuels. Reiter and Kong [38], who carried out tests in a CI engine by injecting ammonia in the intake pipe (PFI), found that soot decreased significantly with increasing ammonia while NO_x reduced up to 40% ammonia content because of the lower flame temperature. Their results showed a much more delayed combustion process for increasing ammonia amounts. Similar results were obtained in the computational work carried out by Boretti [39].

Methane, both neat and in the form of natural gas, has been assayed from several years ago as a low reactive fuel, as described in the review of Sahoo et al. [40]. Hernández et al. [41] proved dual-fuel combustion to be characterized by a higher brake specific fuel consumption than conventional diesel operation due to the lower heating value of methane as well as to the unburnt methane (mainly at low engine loads). In addition, this work also showed that, for the diesel fuel replacements tested (up to 40% by energy), the autoignition time was not affected by methane. Similar conclusions were obtained by Mancaruso et al. [42] in an optical CI engine. The lower adiabatic flame temperature of methane has also been reported to decrease NOx emissions under CI dual-fuel combustion mode [41].

In this work, the autoignition behaviour of diesel fuel under dual operation with H_2, NH_3 and CH_4 (the latter two considered as e-fuels) has been analysed. As mentioned before, several works can be found in literature dealing with this topic (mainly for methane), but most of them were carried out in engines (usually under very different operating conditions) and focused on performance and emissions rather than on an exhaustive analysis of a particular phenomenon. In this work, experiments were carried out in a constant volume combustion chamber (CVCC), typically used to measure the derived cetane number (DCN) of diesel-type fuels [43]. This device allows for a more comprehensive evaluation of autoignition (under very well-controlled conditions) since it avoids the uncertainties derived from cycle-to-cycle and volume variations in an engine, as well as the very relevant impact of the in-cylinder turbulence. It therefore prevents non-fuel effects and facilitates the comparison between the three LRFs (which, to the authors' knowledge, has not been done before). Furthermore, because of the evolution of low-temperature combustion modes, in which chemical processes would

seem to behave in a capricious manner, having experimental data at temperatures such as those tested in this work under dual operation may be valuable for validating/developing chemical kinetics mechanisms to be used in computational codes.

2. Methodology and experimental setup

This section describes the experimental device as well as the methodology used (experimental conditions tested). As mentioned below, the procedure followed tried to keep the same global equivalence ratio in the combustion device in order to isolate the effect of the fuel on the autoignition phenomena from that of the oxygen availability.

2.1. Fuels

Diesel fuel (D) was used as high reactivity fuel. It was supplied by Repsol, with no oxygen content. On the other hand, methane (CH_4), ammonia (NH_3) and hydrogen (H_2) were used as gaseous fuels. They were named as low reactivity fuels (LRFs) when describing general features for all of them. Table 1 shows the main properties of these fuels.

2.2. Experimental procedure

Experimental tests were carried out in a Herzog Cetane ID510, which consists of a 0.473 L constant volume combustion chamber equipped with a common rail diesel injector (operating at 1000 bar injection pressure), widely described in previous works [45,46]. Before performing the fifteen injection events (which are averaged) used to determine the combustion related information from the instantaneous pressure signal (delay time, derived cetane number as defined in the standard ASTM D6117 [43] etc.), the device carries out five pre-injections to clean the chamber out of residual fuel from previous tests. The experimental procedure was described in [33]. Before the injection of the diesel fuel, the chamber was fed with a mixture of synthetic air and the gas under study (H_2, NH_3 or CH_4) and held in during approximately one minute to reach the defined temperature setpoint. The gas concentration in the bottles was calculated considering the desired energy replacements for the diesel fuel. The injection pulse width used for conventional operation (only diesel) was 2500 μs, as established in [43], this duration being shortened when diesel fuel was replaced by gas. Because of the significant effect of the equivalence ratio (*Fr*, defined as the fuel/air mass ratio with respect to the stoichiometric one) on the ignition delay time, this was kept constant when substituting diesel fuel with gas (Tables 2 to 4), with slight deviations with the chamber temperature (which influences the amount of the introduced air/gas mixture). However, and because of limitations of the device (maximum injection duration of 3000 μs), the equivalence ratio was quite lower (although very similar for all the replacements) when decreasing the vessel pressure. The autoignition delay times are defined as suggested in Lapuerta et al. [47]. With regards to the cool flame, this time (ID_{CF}) is the elapsed time from the start of injection to the instant at which pressure rises 0.2 bar above the initial pressure (provided that a two-stage autoignition behaviour was observed in the dp/dt diagram), while the main combustion timing (ID_M) is identified as the instant at which the line connecting 1/2 and 1/4 of the rates of pressure (dp/dt) equals zero. In case autoignition involves only one stage, the ignition delay is identified as the ID_M previously commented.

A fraction of the energy provided by the diesel fuel was progressively replaced by energy provided by the LRF following Equation (1) (as also done by other authors [3,47]),

$$E_{LRF}(\%) = 100.\frac{m_{\mathrm{LRF}}.LHV_{\mathrm{LRF}}}{m_{\mathrm{LRF}}.LHV_{\mathrm{LRF}} + m_{\mathrm{D}}.LHV_{\mathrm{D}}} \quad (1)$$

where E_{LRF} is the LRF energy share ratio (in percentage), m_{LRF} y m_{D} are the LRF and diesel fuel mass respectively and LHV_{LRF} and LHV_{D} the corresponding lower heating values. As shown in Tables 2 to 4, three different energy replacement levels (approximately 10, 20 and 40%) were achieved, trying to keep constant the total energy into the chamber. Substitutions of approximately 40% H_2 were not possible since synthetic bottles of H_2/air mixture at the required concentration (4% by mol.) were not available from the supplier for safety reasons. Each combination was tested at three initial temperatures, T_0 (535, 600 and 650 °C) for an initial pressure (p_0) of 21 bar, and at three initial pressure values (11, 16 and 21 bar) for an initial temperature of 600 °C. As previously mentioned, the different initial chamber temperature led to marginal variations in the equivalence ratio between 0.36 and 0.42 (as shown in Tables 2 to 4). This ratio remained around 0.8, 0.5 and 0.4 for p_0 equals to 11, 16 and 21 bar, respectively.

Tables 2 (replacements with H_2), 3 (replacements with NH_3) and 4 (replacements with CH_4) show the results obtained for ID_{CF}, ID_{M}, peak pressure ($p_{\max}$) and maximum pressure gradient (dp/d$t_{\max}$) for all tests as a function of E_{LRF}, together with the most relevant experimental conditions (diesel fuel injection duration, Δt_{inj}, and initial chamber pressure and temperature, p_0 and T_0 respectively). These results are commented and described in the following sections. The 95% confidence limits values according to Student's t-distribution based on the 15 cycles recorded for each condition were also included. As observed, deviations are small with respect to the change in the mean *ID* values, confirming the relevance of the trends discussed below.

Table 1
Properties of the fuels tested.

Property	Method	Diesel	H_2	NH_3	CH_4
C (% m/m)	EN ISO 16948	86.41 [a]	~	~	74.87
H (%m/m)	EN ISO 16948	13.5 [a]	100	17.76	25.13
O (%m/m)	EN ISO 16948	0 [a]	~	~	~
N (%m/m)		~	~	82.24	~
Density at 15.0C (kg/m^3)		842 [a]	~	~	~
Lower heating value (MJ/kg)	UNE 51123	42.90 [a]	120[b]	18.8[b]	50[b]
Derived cetane number	ASTM D7668	51.95 [a]	~	~	~
Stoichiometric fuel/air ratio	N/A	1/14.5	1/34.33	1/6.05	1/17.41
Flammability limits (gas in air) (vol. %) [c]	~	0.6–7.5	4–75	16–25	5–15
Autoignition temperature (K) [c]	~	503	844	924	723
Molecular weight (kg/kmol)	N/A	203.08	2.02	17.03	16.04
H/C ratio	N/A	1.83	~	~	~

[a] Measured
[b] Taken from NIST Chemistry WebBook [44].
[c] Taken from Dimitriou et al. [7].

3. Results and discussion

This section shows the main results regarding the autoignition process of the fuels tested as well as the theoretical kinetics analysis, the latter carried out to highlight the chemical effect of the LRF as well as to identify the reasons for the proved chemical competition with the diesel fuel.

3.1. Combustion development and ignition delay time

Fig. 1 shows the averaged pressure trace obtained from the 15 individual pressure signals at 21 bar. The colour of the curves relates to the initial temperature (650 °C in red, 600 °C in green and 535 °C in blue) while the thickness refers to the proportion of LRF replacing the diesel fuel. The dashed lines correspond to $E_{\mathrm{LHR}} = 0$ (i.e., neat diesel), and must be considered as a baseline. Despite of the importance of the conditions

Table 2
Results (average ± 95% confidence interval) for H_2 at different p_0 and T_0 values.

p_0 (bar)	T_0 (°C)	Δt_{inj} (ms)	Equivalenceratio (Fr)	E_{LRF} (%)	ID_{CF} (ms)	ID_M (ms)	p_{max} (bar)	dp/dt_{max} (bar/ms)
21	535	2500	0.36	0.00	5.92 ± 0.10	7.52 ± 0.13	42.39 ± 0.06	14.15 ± 1.16
21	535	2224	0.36	11.04	5.80 ± 0.06	7.85 ± 0.09	41.73 ± 0.08	10.08 ± 0.62
21	535	1948	0.36	22.07	5.76 ± 0.05	8.33 ± 0.13	41.27 ± 0.13	7.37 ± 0.62
21	600	2500	0.39	0.00	2.36 ± 0.03	3.61 ± 0.06	40.96 ± 0.10	39.15 ± 2.48
21	600	2245	0.39	10.19	2.44 ± 0.01	3.72 ± 0.02	40.09 ± 0.09	32.80 ± 1.09
21	600	1989	0.39	20.37	2.36 ± 0.01	3.74 ± 0.04	38.75 ± 0.25	25.97 ± 1.16
21	650	2500	0.41	0.00	1.84 ± 0.01	2.74 ± 0.02	40.04 ± 0.09	34.84 ± 2.08
21	650	2258	0.41	9.66	1.88 ± 0.01	2.87 ± 0.03	38.30 ± 0.10	32.95 ± 2.05
21	650	2017	0.41	19.32	1.88 ± 0.02	2.90 ± 0.02	36.78 ± 0.08	27.83 ± 1.73
16	600	2447	0.50	0.00	2.48 ± 0.02	4.30 ± 0.03	34.99 ± 0.14	39.82 ± 1.30
16	600	2247	0.50	7.76	2.60 ± 0.01	4.48 ± 0.02	34.58 ± 0.11	33.53 ± 0.81
16	600	2049	0.50	15.52	2.52 ± 0.02	4.59 ± 0.04	33.65 ± 0.13	25.58 ± 1.15
11	600	2691	0.80	0.00	2.72 ± 0.02	5.52 ± 0.03	31.90 ± 0.23	46.70 ± 1.60
11	600	2540	0.80	5.34	2.96 ± 0.01	5.80 ± 0.03	30.89 ± 0.16	40.53 ± 1.08
11	600	2390	0.80	10.67	2.96 ± 0.02	5.98 ± 0.03	30.07 ± 0.15	34.65 ± 1.42

Table 3
Results (average ± 95% confidence interval) for NH_3 at different p_0 and T_0 values.

p_0 (bar)	T_0 (°C)	Δt_{inj} (ms)	Equivalenceratio (Fr)	E_{LRF} (%)	ID_{CF} (ms)	ID_M (ms)	p_{max} (bar)	dp/dt_{max} (bar/ms)
21	535	2500	0.36	0.00	5.92 ± 0.10	7.52 ± 0.13	42.39 ± 0.06	14.15 ± 1.16
21	535	2239	0.36	10.43	5.72 ± 0.07	7.89 ± 0.09	42.97 ± 0.07	9.28 ± 0.56
21	535	1952	0.36	21.91	5.72 ± 0.06	9.15 ± 0.35	43.67 ± 0.17	5.78 ± 0.49
21	535	1457	0.37	41.73	5.16 ± 0.04	13.80 ± 0.78	43.53 ± 0.31	2.19 ± 0.16
21	600	2500	0.39	0.00	2.36 ± 0.03	3.61 ± 0.06	40.96 ± 0.10	39.15 ± 2.48
21	600	2259	0.39	9.63	2.44 ± 0.02	3.86 ± 0.03	40.84 ± 0.08	31.59 ± 1.80
21	600	1994	0.39	20.22	2.52 ± 0.02	4.18 ± 0.03	41.06 ± 0.15	21.25 ± 1.24
21	600	1537	0.40	38.52	2.48 ± 0.01	4.33 ± 0.05	40.06 ± 0.38	9.53 ± 0.81
21	650	2500	0.41	0.00	1.84 ± 0.01	2.74 ± 0.02	40.04 ± 0.09	34.84 ± 2.08
21	650	2272	0.41	9.13	1.92 ± 0.02	2.88 ± 0.04	39.49 ± 0.15	32.23 ± 2.11
21	650	2020	0.42	19.18	2.00 ± 0.02	3.18 ± 0.04	39.42 ± 0.14	28.41 ± 0.84
21	650	1587	0.42	36.54	2.04 ± 0.01	3.30 ± 0.03	38.32 ± 0.25	17.25 ± 1.45
16	600	2447	0.50	0.00	2.48 ± 0.02	4.30 ± 0.03	34.99 ± 0.14	39.82 ± 1.30
16	600	2244	0.50	7.34	2.60 ± 0.02	4.66 ± 0.03	35.26 ± 0.16	30.96 ± 1.00
16	600	2025	0.50	15.41	2.72 ± 0.02	5.11 ± 0.05	35.24 ± 0.10	18.84 ± 1.20
16	600	1650	0.50	29.35	2.64 ± 0.02	5.63 ± 0.08	34.52 ± 0.13	8.95 ± 0.66
11	600	2691	0.80	0.00	2.72 ± 0.02	5.52 ± 0.03	31.90 ± 0.23	46.70 ± 1.60
11	600	2541	0.80	5.04	3.04 ± 0.01	6.10 ± 0.05	31.07 ± 0.22	38.33 ± 1.57
11	600	2379	0.80	10.59	3.20 ± 0.02	6.77 ± 0.03	30.95 ± 0.14	29.69 ± 1.24

Table 4
Results (average ± 95% confidence interval) for CH_4 at different p_0 and T_0 values.

p_0 (bar)	T_0 (°C)	Δt_{inj} (ms)	Equivalenceratio (Fr)	E_{LRF} (%)	ID_{CF} (ms)	ID_M (ms)	p_{max} (bar)	dp/dt_{max} (bar/ms)
21	535	2500	0.36	0.00	5.92 ± 0.10	7.52 ± 0.13	42.39 ± 0.06	14.15 ± 1.16
21	535	2233	0.36	10.69	5.72 ± 0.09	7.75 ± 0.13	42.53 ± 0.09	11.05 ± 0.98
21	535	1959	0.37	21.64	5.60 ± 0.07	8.05 ± 0.13	43.07 ± 0.14	8.06 ± 0.46
21	535	1392	0.37	44.32	5.28 ± 0.05	9.44 ± 0.61	44.11 ± 0.22	3.90 ± 0.37
21	600	2500	0.39	0.00	2.36 ± 0.05	3.61 ± 0.10	40.96 ± 0.10	39.15 ± 2.48
21	600	2253	0.39	9.86	2.36 ± 0.03	3.72 ± 0.06	39.56 ± 0.12	33.10 ± 1.37
21	600	2001	0.40	19.97	2.32 ± 0.02	3.77 ± 0.05	37.73 ± 0.08	24.27 ± 2.02
21	600	1477	0.40	40.90	2.24 ± 0.01	3.98 ± 0.05	33.64 ± 0.08	8.80 ± 1.09
21	650	2500	0.41	0.00	1.84 ± 0.02	2.74 ± 0.03	40.04 ± 0.09	34.84 ± 2.08
21	650	2266	0.41	9.36	1.88 ± 0.02	2.87 ± 0.03	38.47 ± 0.10	32.54 ± 2.41
21	650	2026	0.42	18.94	1.92 ± 0.03	3.01 ± 0.17	36.76 ± 0.09	27.67 ± 2.30
21	650	1530	0.42	38.80	1.92 ± 0.02	3.28 ± 0.06	33.51 ± 0.09	14.98 ± 3.24
16	600	2447	0.50	0.00	2.48 ± 0.04	4.30 ± 0.05	34.99 ± 0.14	39.82 ± 1.30
16	600	2242	0.50	7.52	2.56 ± 0.03	4.54 ± 0.04	34.21 ± 0.14	31.36 ± 1.72
16	600	2034	0.50	15.22	2.52 ± 0.03	4.63 ± 0.06	32.79 ± 0.09	22.63 ± 0.96
16	600	1602	0.50	31.16	2.48 ± 0.02	5.19 ± 0.10	29.89 ± 0.13	8.28 ± 0.45
11	600	2691	0.80	0.00	2.72 ± 0.03	5.52 ± 0.05	31.90 ± 0.23	46.70 ± 1.60
11	600	2546	0.80	5.17	3.00 ± 0.03	5.92 ± 0.04	30.46 ± 0.16	37.85 ± 0.98
11	600	2399	0.80	10.46	3.00 ± 0.03	6.08 ± 0.06	29.17 ± 0.10	31.37 ± 1.02
11	600	2094	0.80	21.84	3.00 ± 0.01	7.13 ± 0.07	27.73 ± 0.15	20.80 ± 1.13

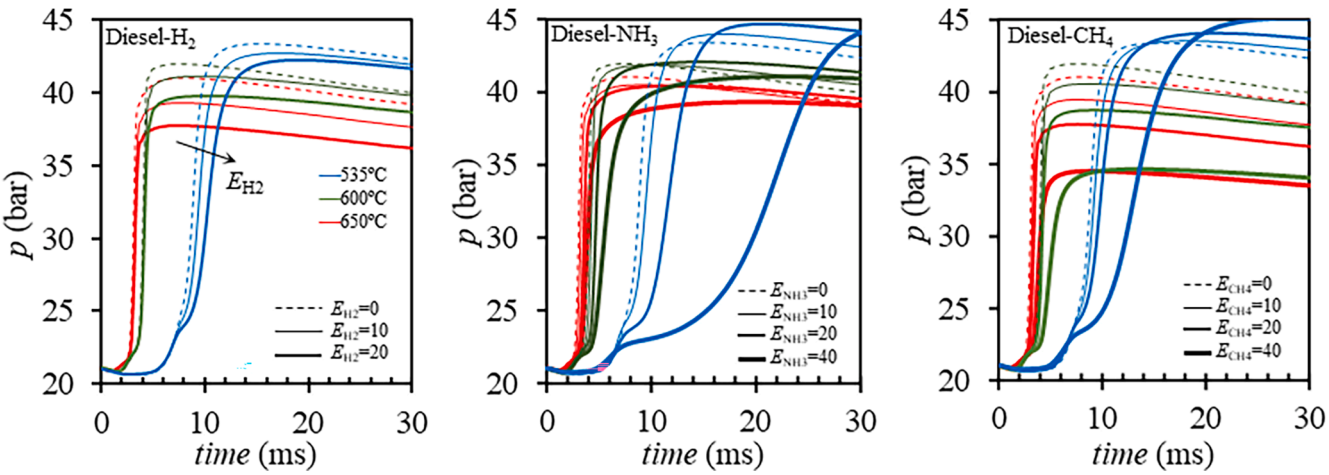

Fig. 1. Instantaneous pressure evolution for different replacements with H_2 (~10 and 20%, left), NH_3 (~10, 20 and 40%, center), and CH_4 (~10, 20 and 40%, right) at p_0 = 21 bar and T_0 = 535 °C (blue), 600 °C (green) and 650 °C (red).

at the time of the diesel fuel injection (T_0, p_0, F_r) on the eventual autoignition process, the content and nature of the low-reactivity fuel also play a very significant role under dual combustion mode. For all the cases, the typical two-stage autoignition behaviour (cool flames and main combustion) of alkanes (>C4-C5) under low-intermediate temperature was detected. Since none of the LRFs exhibit negative temperature coefficient (NTC) behaviour under the conditions studied, the low-temperature heat release seems to be exclusively dominated by the diesel fuel, the LRF not significantly affecting neither the intensity nor the timing of the cool flame event. However, the main combustion phasing is quite sensitive to the presence of the LRF (more evident at the lower initial temperature, for which autoignition is largely deferred).

The commented insights can be more easily deduced from Fig. 2, which shows the ID_{CF} and ID_M at 21 bar. These results are in agreement with those obtained by Boretti [13,39] in a diesel engine operating under dual mode with different gases. While the effect of hydrogen and methane on the autoignition onset was very similar, ammonia was the gaseous fuel inhibiting the combustion development in a greater extent. This effect was more noticeable at the lowest chamber temperature, for which the fuel oxidation kinetics plays a more important role. A more detailed analysis on the kinetics effect of the LRF is presented in Section 3.2.

Fig. 3 displays, as an example, the instantaneous pressure gradient for the three low reactivity fuels at 600 °C (similar trends were observed for the rest of conditions tested). As observed, the combustion rate slowed down as the LRF content increased because of very leaner fuel/air mixtures at the ignition event (derived from higher ignition delay times). Moreover, a "M−shaped peak" pattern can be clearly detected. This should not be confused with the typical diesel fuel premixed phase preceding diffusive combustion under conventional diesel conditions, as the maximum injection time does not exceed 2.5 ms in any case (much earlier than the appearance of the M−shaped peak). As stated in the work of Ahmad et al. [48] carried out in an optical CI engine with methane, the first stage could correspond to the combined combustion of the diesel fuel and the entrained LRF in the diesel plume, while the second stage might be caused by the oxidation of the remaining LRF through flames propagating from the diesel jets. These conclusions have also been reported in the review of Sahoo et al [40] for the same LRF fuel (methane). However, due to the high ignition delays under the conditions tested (clearly leading to uncoupled injection-combustion events) as well as to the extremely lean LRF/air mixture (limiting flame propagation), the observed two peaks are suggested to correspond with a highly premixed (and spatially distributed) autoignition of the diesel fuel and the entrained LRF, followed by the autoignition of the remaining LRF around the diesel ignition kernels. This explanation is in agreement with the findings of Rochussen et al. [49] obtained in a 2 L single-cylinder engine operating under dual mode at low load conditions. The commented pattern was observed for the three LRFs in the present work. It is remarkable to observe the overlapping between both combustion regimes for the highest proportion of the LRF, also reported by Ahmad et al. [48], in agreement with the higher amount of entrained LRF in the diesel jets because of the more delayed ignition.

As also observed in the previous figures, replacements with LRF also lead to a reduction of the peak pressure. This is due to several factors.

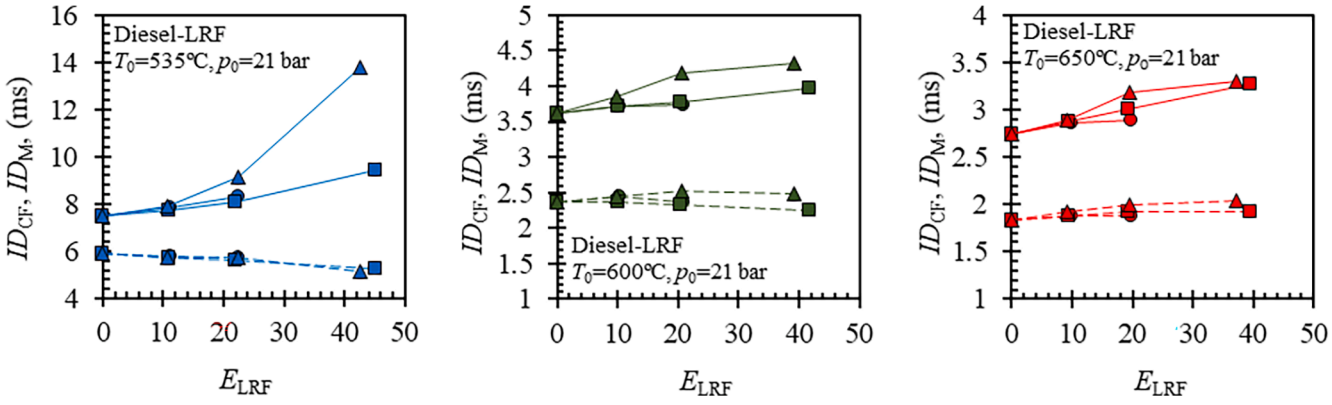

Fig. 2. Ignition delay times (ID_{CF}: dashed lines, ID_M: solid lines) for different replacements with hydrogen (●), ammonia (▲) and methane (■) at p_0 = 21 bar and T_0 = 535 (left), 600 (center) and 650 °C (right).

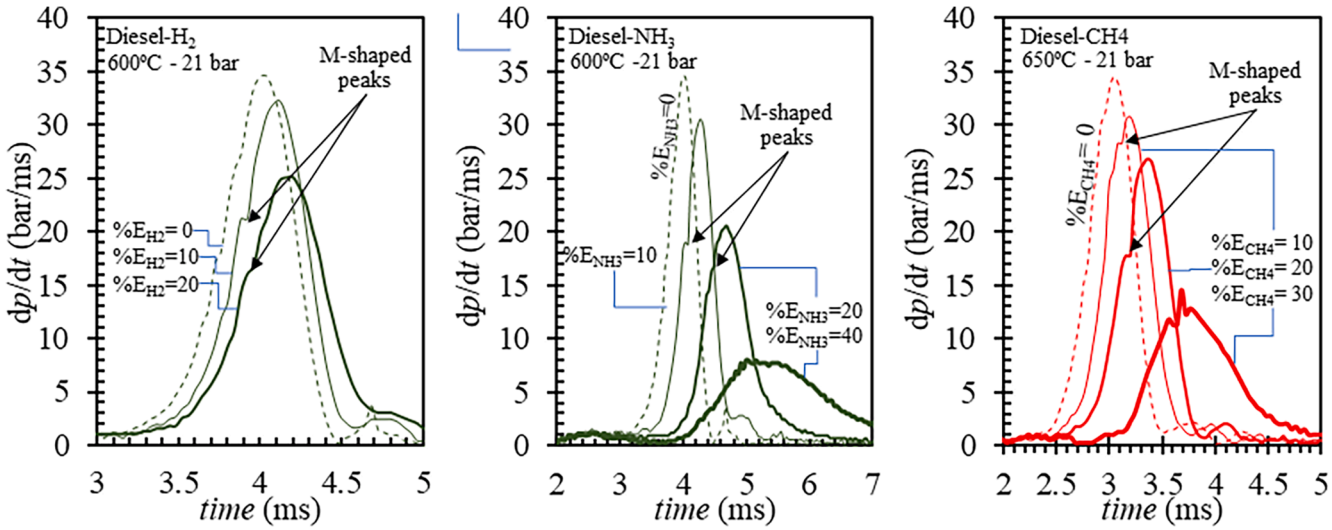

Fig. 3. Selected dp/dt curves for different replacements with H_2 (left), NH_3 (center), and CH_4 (right).

Firstly, to the unburned gaseous fuel which is close to the combustion chamber walls. As the LRF/air mixture is too lean, the colder gaseous fuel far away from the diesel fuel jet is unlikely to react. This explains that the relative reduction in the peak pressure with the LRF content was more significant for methane, since its lower flammability limit is greater than that of hydrogen and ammonia [7]. Secondly, the molecular expansion of the combustion products with respect to the reactants is lower for the LRF, which also affects the pressure evolution [50]. The effect of the LRF on the maximum pressure seems to be compensated at 535 °C because of the longer ignition delay time, promoting a greater entrainment of the gas into the liquid jet, and thereby reducing the amount of unburned LRF. Moreover, despite of keeping a similar energy content when changing the operating conditions and the type of LRF, lower initial chamber temperatures led to higher peak pressures. Since the injector is located inside the chamber, this might be due to the lower diesel fuel density. So, small variations in the amount of injected liquid fuel are expected when changing the chamber temperature since not the liquid mass but the volume was kept constant.

Fig. 4 shows the results obtained at different initial pressures (11, 16 and 21 bar) while keeping the initial temperature at 600 °C. Lower pressure reduces the probability of collision between molecules, which results in a decrease in reactivity. This was reflected through the displacement of the autoignition delay time to higher values as p_0 decreases. It is remarkable that the timing of cool flames is much weaker pressure-sensitive than that of the main combustion. Since pressure-dependant reactions are usually those regarding unimolecular recombination paths (involving a third body), the low thermal level existing in the NTC region does not allow for the occurrence of these reactions and thus cool flames are not limited by pressure [37]. The pressure trace follows very similar trends with the diesel fuel replacement (a delay on the autoignition for the higher replacements) for all the initial pressure values tested.

3.2. Kinetics analysis

Validation of theoretical data coming from kinetics models assuming homogeneity with experimental data obtained in the CVCC used in this work is not evident. Since this chamber mimics a diesel engine fuel injection, the fuel is fed as a liquid and therefore not only a chemical but also a physical (atomization, evaporation and air entrainment phenomena) delay is involved on autoignition (the latter having a more significant relative weight when the chamber temperature and/or pressure increases). Consequently, inhomogeneities are present (richer and poorer zones), which gradually disappear as the mixing progresses. However, using a Closed Homogeneous Reactor, as that considered in this work by using the CHEMKIN package [51], is valuable for a better understanding of the LRF chemical interactions on the diesel fuel reaction paths. In general, a simulation under similar CVCC conditions is

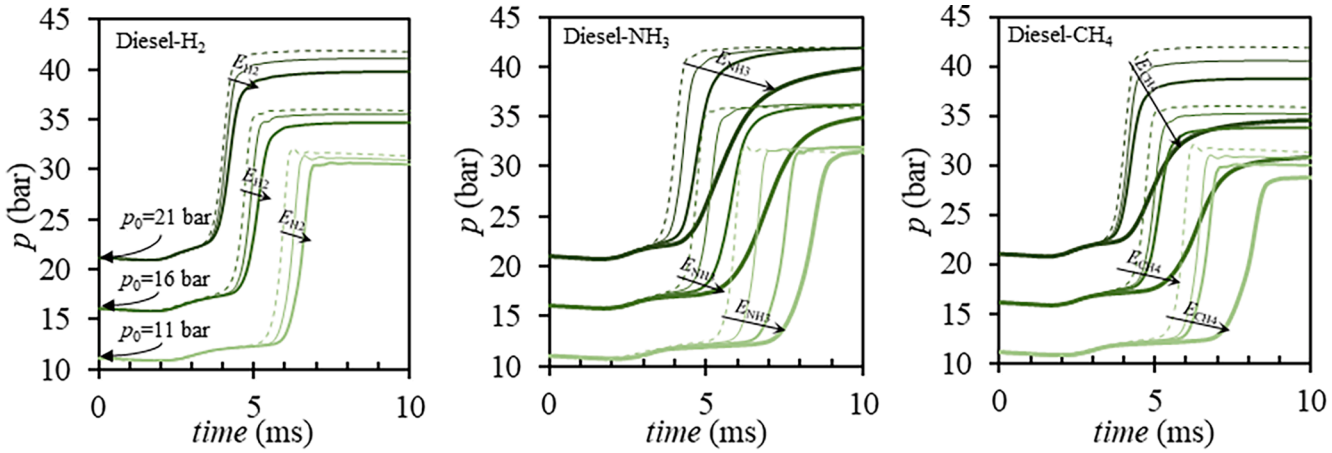

Fig. 4. Instantaneous pressure evolution for different replacements with H_2 (~0, 10 and 20%, left), NH_3 (~0, 10, 20 and 40%, center), and CH_4 (~0, 10, 20 and 40%, right) at T_0 = 600 °C and p_0 = 11, 16 and 21 bar.

likely to underestimate the autoignition delay time. Such deficiencies could be partially overcome by CFD modelling coupled to chemical kinetics, as done by Luecke et al. [52] in a similar device (AFIDA, Advanced Fuel Ignition Delay Analyser). However, for sake of simplicity and because of autoignition was much longer than the injection duration for all cases (the latter was shorter than 2.5 ms, as shown in Section 2.2, while the minimum ID_M was 3.61 ms), the assumption of homogeneity at the ignition event could be accurate enough (mainly for the higher replacements with the LRF and the lower chamber temperatures because of the very delayed ignition).

For modelling the diesel fuel oxidation, a three-component surrogate (consisting of n-hexadecane ($nC_{16}H_{34}$, 41.3% mol), isocetane ($iC_{16}H_{34}$, 36.8% mol) and 1-methylnaphthalene ($C_{10}H_7CH_3$, 21.9% by mol)), already used by other authors [37,53] and proposed by Qian et al. [54], together with the chemical kinetic mechanism developed by CRECK (consisting of 201 species and 4417 reactions), were used [55]. As known, H_2 and CH_4 are part of the core C_0-C_4 mechanisms, therefore no additional reactions were required for their consideration. In the case of NH_3, the model proposed by Stagni et al. [56], consisting of 31 species and 203 reactions, was added to that of the diesel fuel. This is a recent and comprehensive mechanism, proposed to improve the modelling of ammonia oxidation and pyrolysis at low temperatures and fuel-lean conditions [22]. Both diesel fuel and NH_3 mechanisms were merged using the Ansys Workbench Reaction tool, obtaining a combined chemical kinetic mechanism of 222 species and 4598 reactions. For the sake of simplicity, it was assumed that the interaction between the two mechanisms is constrained to the effects of sharing common radical pools [57], therefore possible co-oxidation reactions were not considered.

Fig. 5 shows the theoretical history of pressure and mole fraction of selected species (fuel components and •OH radical, the latter being recognized as the most representative ignition compound) as the energy substitution was increased from 0 (pure diesel) to 10, 20 and 40%. As expected from the reactivity of the pure components (maximum for paraffins and very low for the LRFs), n-hexadecane (the linear paraffinic of the diesel fuel) exhibited the highest consumption rate, while *iso*-cetane (the branched alkane) and, at a lower rate, 1-methylnaphthalene (the aromatic fraction) were consumed slowly. As observed, the concentration of the gaseous fuel (LRF) remained almost unchanged up to the autoignition event. This sequence has been highlighted by the yellow circle of the diesel-NH_3 combination (Fig. 5-middle), in which the colour arrows refer to the previously mentioned components. The commented trend is consistent with the fact that the reactions initiating the oxidation process at low temperature are the H_2-abstraction ones, which are characteristic of paraffins. Cool flames were more pronounced for low LRF ratios (as confirmed by the •OH radical peaks appearing during the first 2 ms), confirming once again (coherently with the experimental results) the dominant role of the diesel fuel on the low temperature

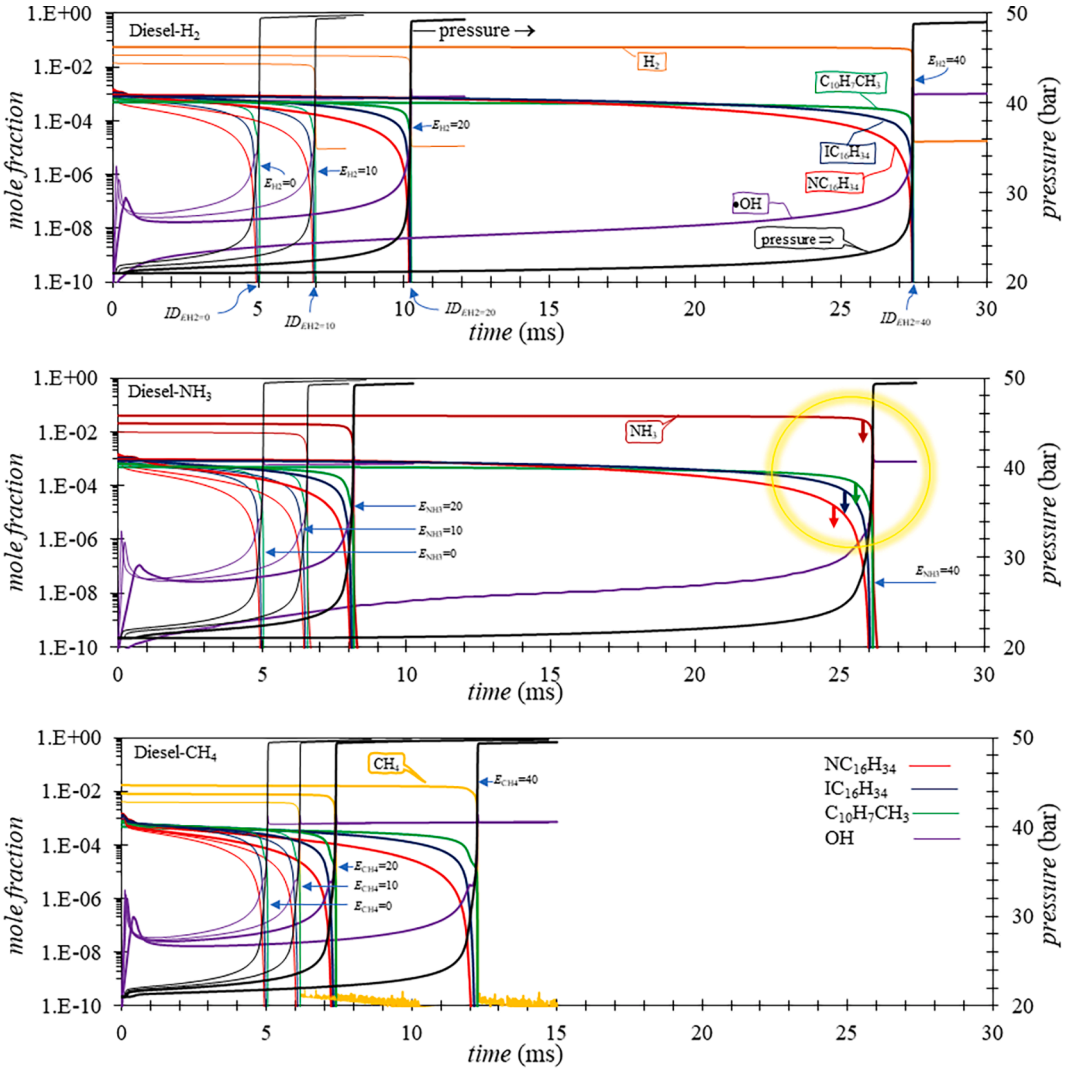

Fig. 5. Time-profile for the OH radical, the diesel fuel constituents ($nC_{16}H_{34}$, $iC_{16}H_{34}$, $C_{10}H_7CH_3$) and the three LRF for different replacements with H_2 (top), NH_3 (medium) and CH_4(bottom) at p_0 = 21 bar and T_0 = 600 °C.

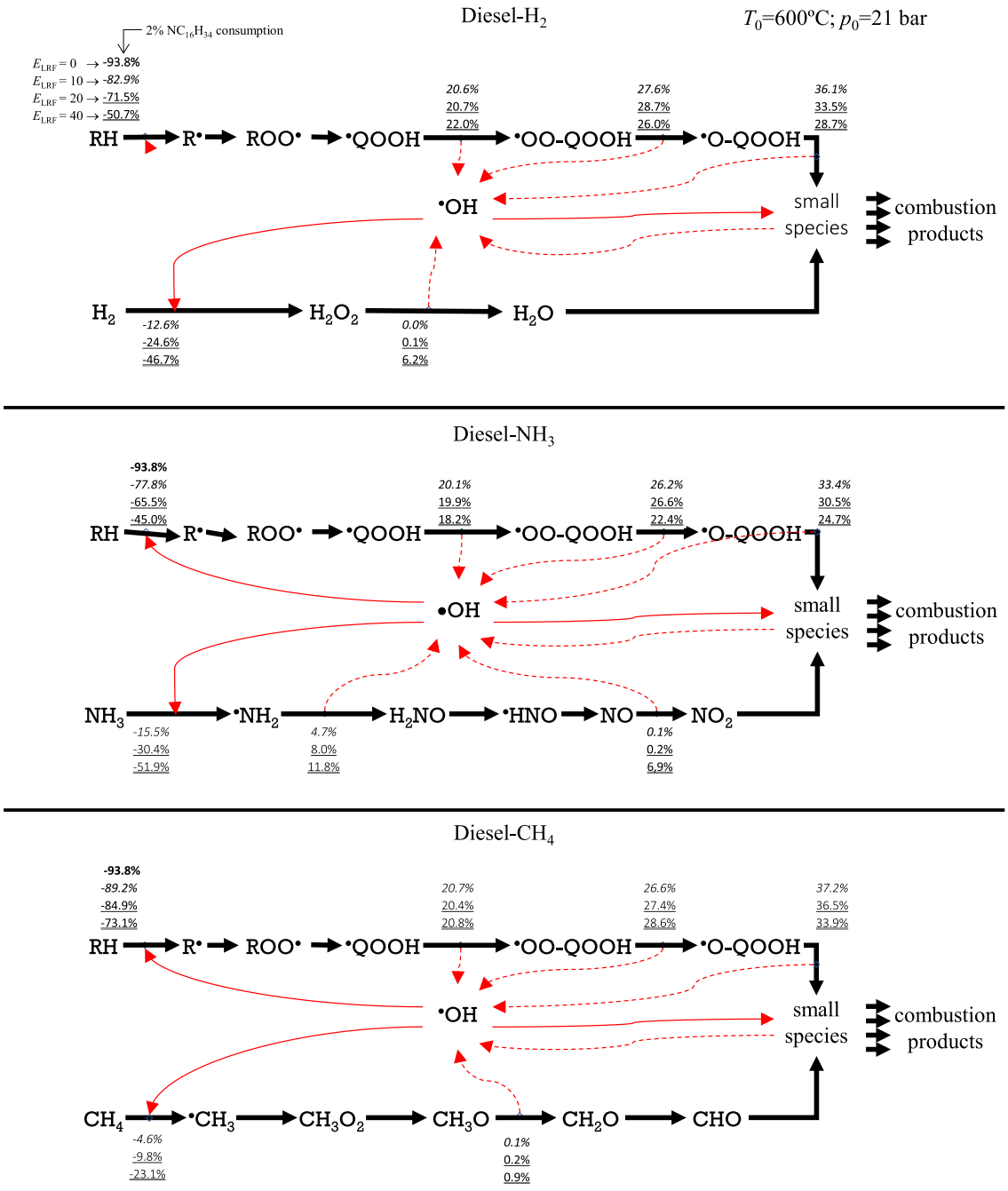

Fig. 6. Comparison of simplified reaction pathways at 2% consumption of $nC_{16}H_{34}$ for 10% (italics), 20% (underlined) and 40% (double underlined) replacements (p_0 = 21 bar, T_0 = 600 °C).

oxidation regime. This indicates that the main supplier of •OH radical is the diesel fuel. The LRFs' marginal consumption of •OH (as described in the following section) might also contribute to this trend.

Fig. 6 shows the competition for •OH between diesel fuel (represented by RH) and each of the three LRFs (H_2, NH_3 and CH_4) at a specific instant of the oxidation process. Each reaction pathway was constructed to emphasise such competition at the start of the reactive process. Data were obtained by carrying out a Rate of Production (ROP) analysis of OH radicals by means of the CHEMKIN software. The numbers presented in boxes corresponds to different energy replacements with the LRF (0% bold, 10% italics, 20% underlined and 40% double underlined). Number corresponds to data at the beginning of the diesel fuel oxidation process (supposed as 2% conversion of n-Hexadecane). Selected general reactions for both fuels were represented, merging into a pool of smaller molecules that ultimately lead to combustion end products. In the centre of the schemes, the •OH radical pool is shown separately with arrows leading in and out of it. The solid red lines refer to •OH radical consumption by the reaction to which the arrow points. The dashed red lines indicate •OH radical production by the reactions from which the arrow originates. In the case of diesel fuel, RH represents the set of the three fuel components (i.e., $nC_{16}H_{34}$, $iC_{16}H_{34}$ and $C_{10}H_7CH_3$), so that •OH consumption and production are not discriminated for each component but treated as one. Hence, any intermediate specie should be understood as the total contribution of those components (i.e., ROO•: nC_{16}-OQOOH, iC_{16}-OQOOH).

The oxidation kinetics may be summarized this way. At low

temperature, the fuel molecule RH is predominantly consumed through H-abstractions by •OH [58,59] (and to a much lesser extent by other species such as O_2), leading to the production of alkyl radicals (R•). These radicals are further consumed by a first O_2 addition, producing ROO•, leading to hydroperoxyalkyl (•QOOH) radicals by internal H-abstraction via five-, six-, or seven-membered transition state rings (isomerization processes). Thus, another O_2 molecule is added to the radical site, forming peroxyhydroperoxyalkyl radical (•OOQOOH). This leads to ketohydroperoxide formation (•OQOOH). The latter path is the main •OH producer and it identifies the low temperature branching scheme [60,61], Eventually, the decomposition of these species degenerates into smaller species (aldehydes, ketones, etc.). In parallel, the LRF is oxidized at a much slower rate (see Fig. 5), and its intermediates and oxidation products flow into the same pool of smaller molecules, to finally produce combustion products (CO, CO_2, H_2O, etc.).

The effect of replacing diesel fuel by the LRF on the relative consumption of the main active radical (•OH) is evident. In the case of H_2, 93.8% of the •OH is consumed by H-abstraction from the RH for pure diesel fuel. Regardless of the rest of the reaction scheme, this is the key step for the chemical interaction between both fuels [9]. With E_{H2} of 10, 20 and 40%, this percentage drops to 82.9, 71.5 and 50.7, respectively. Moreover, the production of •OH, mainly via decomposition of •OOQOOH and •OQOOH, is reduced from 36.1% to 33.5% and 28.7%, respectively. This reduction in the OH formation has also been reported in the work of Zhu et al. for methane [62]. This proves that the presence of H_2 reduces the •OH availability for the diesel fuel decomposition, which is ultimately responsible of autoignition. Consequently, this results in higher ignition delay times. The data for NH_3 (77.8, 65.5 and 45 %) and CH_4 (89.2, 84.9 and 73.1%) regarding H-abstraction reactions also reveals a great effect of ammonia, which demands a high proportion of •OH, and a minor influence of CH_4 on the autoignition time. These findings are, in general, in agreement with the experimental data described in Section 3.1, although kinetics simulations showed more delayed autoignition processes for H_2 than for NH_3. Similar conclusions can be obtained from the LRF point of view (numbers at the bottom of each scheme), an increase in E_{LRF} results in a higher fraction of •OH consumed by itself (again less significant for CH_4).

Although the chemical effect of the LRF on the autoignition process has been proved above, there are other phenomena which may also modify the ignition timing (physical effect), such as those derived from the different thermal and diffusive properties of the charge because of the presence of the LRF. To isolate both effects and highlight the role of kinetics for each gaseous fuel (LRF), additional modelling efforts were undertaken at $p_0 = 21$ bar and $T_0 = 600$ °C. A decoupling method in which simulations were performed by assigning the thermodynamic and transport properties of each LRF to an inert compound was used. Specifically, the content of the LRF was removed and the thermodynamic and transport properties of argon (Ar, with a concentration equals to that of the LRF) were replaced by those of the LRF, so that Ar is converted into a fictitious and unreactive LRF (denoted as LRF_{ur}). A similar procedure was previously used by Liu [63] and Rezgui [64].

The results are shown in Fig. 7, where green lines represent the original behaviour (considering both the chemical and the physical effect) while the blue line corresponds to the unreactive LRF (LRF_{ur}, without kinetics implications). As expected, the peak pressure values regarding the former are higher because of the energy content of the LRF. For clarity, each LRF/LRF_{ur} pair of curves have been linked with a loop. As observed, and mainly for the higher replacements of diesel fuel (for which differences in the ignition delay are high enough to distinguish the analysed effects), the inert LRF lags autoignition, this delay being more important for NH_3 and much less significant for CH_4. These results agree with the experimental ones (Section 3.1), and they confirm that the LRF chemical effect on autoignition overwhelms that of different physical (thermal and diffusive) characteristics.

3.3. Ignition delay time correlations

Since Henein and Bolt [65] established the potential of an Arrhenius-type equation for modelling ignition delay, many authors have used it for particular purposes, such as Hernandez et al. in the case of paraffinic fuels [66] or Zhang et al. [9] under dual fuyel combustion by using methanol and methane [67]. A modified version was used in this work for estimating ID_M as a function of the energy replacement (E_{LRF}). In addition to the initial thermodynamic conditions such as initial pressure (p_0) and temperature (T_0), the total equivalence ratio (F_r) was considered. For strictly mathematical reasons, E_{LRF} was included as (1-E_{LRF}). This prevents the correlation from leading to unrealistic results when E_{LRF} equals zero. The correlation is shown in Equation (2).

$$ID_M = A^{*}p_0^{b}{*}F_r^{d}{*}(1-E_{LRF})^{e}{*}\exp\left(-\frac{E_a}{R^{*}T_0}\right) \quad (2)$$

The optimal value for all the fitting parameters (A, b, d, e, and E_a), displayed in Table 5, were determined by regression analysis, trying to maximize R^2 (coefficient of determination) and to maximize RMSE (Root Mean Square Error) between experimental and modelled values. It was considered that b and d must be negative, since as pressure and

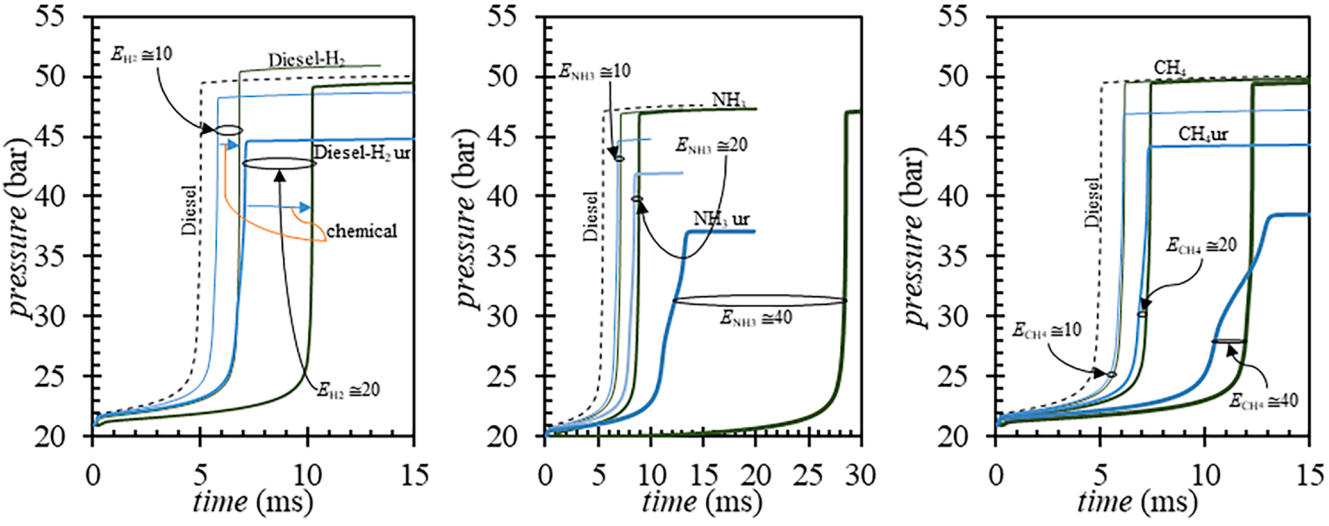

Fig. 7. Pressure traces comparing LRF as a reactive and non-reactive component for different replacements with H_2 (left), NH_3 (center) and CH_4 (right) at $p_0 = 21$ bar and $T_0 = 600$ °C.

Table 5
Fitting parameters for the ID_M correlation.

Parameter	Diesel-H_2	Diesel-NH_3	Diesel-CH_4
A	0.0175	0.0049	0.0182
b	−0.99	−0.99	−0.99
d	−0.32	−0.12	−0.23
e	−0.39	−1.06	−0.43
E_a (J/mol)	58.7	68.4	58.9
RMSE	0.593	4.226	1.671
R^2	0.988	0.970	0.978

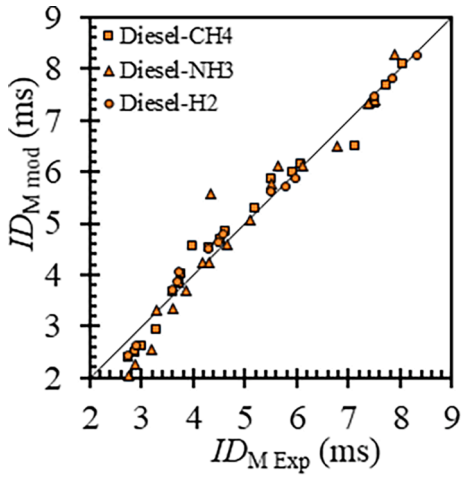

Fig. 8. Parity plot modelled vs experimental ID_M.

equivalence ratio increase (below around the stoichiometric one) the autoignition is advanced.

As checked in Fig. 8, the proposed correlation fitted quite well with the experimental data. However, it is remarkable that the results for ammonia were recurrently further away from the experimental ones, which could be due to a more inaccurate determination of the ID_M value from the pressure traces because of the much smoother pressure increase when compared to hydrogen and methane (derived from very diluted conditions at ignition, leading to a significant low combustion rate).

4. Conclusions

The autoignition behaviour of diesel fuel under dual mode with H_2, NH_3 and CH_4 (for different diesel fuel replacements in an energy basis) has been analysed under well-controlled conditions such as those existing in a constant volume combustion chamber. The main conclusions can be summarized as follows:

- While the influence of the LRF on the cool flame's onset as well as on the low temperature heat release was not significant (this stage being dominated by the liquid fuel), higher LRF energy ratios led to higher delays for the main combustion process.
- The ignition delay time was quite sensitive to the ammonia concentration and mainly at the lowest chamber temperature (535 °C), with a clear non-linear trend.
- Together with the longer autoignition, the combustion duration enlarges with the LRF content because of leaner conditions at the ignition time (more intensified for ammonia due to its low flame speed). Although a higher ignition delay of diesel fuel was expected to be compensated by a shorter combustion duration (derived from a higher premixed combustion phase), the much leaner conditions when autoignition occurs slowed down the combustion development.
- Pressure gradient patterns proved that the diesel fuel and the LRF oxidation process is somehow uncoupled, the combustion rate showing a M−peak shape.
- The analysis of the production/consumption rate of the main active radical (•OH) confirms the chemical interactions between diesel fuel and the LRF regarding H-abstraction reactions (governing the low temperature kinetics regime). This interaction was less important for CH_4, in agreement with the experimental results.
- Kinetics simulations have proved that the chemical effect of the low reactivity fuels is much more significant than that derived from their thermal and diffusive properties (physical effect).
- Instead of highly computational time-demanding reaction mechanisms, the correlations proposed for estimating the main ignition delay for the LRFs tested could be used by CFD codes for simulating CI dual-fuel combustion.

These results suggest the need of important modifications in the injection strategy (timing and events) of CI engines working under dual mode with any of the gases here tested. Moreover, the structural integrity of the engine should not be compromised since pressure gradients were limited by the previously mentioned issue (slower combustion process), unburnt LRF fuel and the lower molecular expansion during the LRF conversion.

CRediT authorship contribution statement

Juan J. Hernández: Conceptualization, Data curation, Formal analysis, Investigation, Methodology, Supervision, Writing – original draft. **Alexis Cova-Bonillo:** Data curation, Formal analysis, Investigation, Writing – review & editing. **Han Wu:** Formal analysis, Investigation, Methodology, Validation. **Javier Barba:** Data curation, Formal analysis, Investigation, Methodology, Validation. **José Rodríguez-Fernández:** Formal analysis, Investigation, Methodology, Writing – review & editing.

Declaration of Competing Interest

The authors declare the following financial interests/personal relationships which may be considered as potential competing interests: Juan J. Hernandez reports financial support was provided by Spain Ministry of Science and Innovation. Juan J. Hernandez reports equipment, drugs, or supplies was provided by Repsol SA.

Acknowledgements

The authors gratefully acknowledge Ministry of Science and Innovation (Spain), for the financial support for the "CO2-dual" project (ref: PID2019-106957RB-C21) and Repsol, for supplying the diesel fuel.

References

[1] Tanaka K, Berntsen T, Fuglestvedt JS, Rypdal K. Climate Effects of Emission Standards: The Case for Gasoline and Diesel Cars. Environ Sci Technol 2012;46(9): 5205–13. https://doi.org/10.1021/es204190w.
[2] Yu X, Sandhu N, Yang N, Zheng M. Suitability of energy sources for automotive application–A review. Appl Energy 2020;271(115169). https://doi.org/10.1016/j.apenergy.2020.115169.
[3] Yang B, Xi C, Wei X, Zeng K, Lai M. Parametric investigation of natural gas port injection and diesel pilot injection on the combustion and emissions of a turbocharged common rail dual-fuel engine at low load. Appl Energy 2015;143: 130–7. https://doi.org/10.1016/j.apenergy.2015.01.037.
[4] Boretti A. Advantages of converting Diesel engines to run as dual fuel ethanol–Diesel. Appl Therm Eng 2012;47:1–9. https://doi.org/10.1016/j.applthermaleng2012.04.037.
[5] Hall C, Kassa M. Advances in combustion control for natural gas–diesel dual fuel compression ignition engines in automotive applications: a review. Renew Sustain Energy Rev 2021;148(111291). https://doi.org/10.1016/j.rser. 2021.111291.
[6] Deheri C, Acharya S, Thatoi D, Mohanty A. A review on performance of biogas and hydrogen on diesel engine in dual fuel mode. Fuel 2020;260(116337). https://doi.org/10.1016/j.fuel.2019.116337.

[7] Dimitriou P, Javaid R. A review of ammonia as a compression ignition engine fuel. Int J Hydrogen Energy 2020;45(11):7098–118. https://doi.org/10.1016/j.ijhydene. 2019.12.209.

[8] Ashok B, Ashok S, Kumar C. LPG diesel dual fuel engine-A critical review. Alexandria Eng J 2015;54(2):105–26. https://doi.org/10.1016/j.aej.2015.03.002.

[9] Zang R, Yao C, Yin V, Geng P, Hu J, Wu T. Mechanistic Study of Ignition Characteristics of Diesel/Methanol and Diesel/Methane dual fuel engine. Energy Fuels 2016;30:8630–7. https://doi.org/10.1021/acs.energyfuels.6b00716.

[10] Sahoo BB, Sahoo N, Saha, UK. Assessment of a Syngas-Diesel Dual Fuelled Compression Ignition Engine. Proceedings of the ASME 2010 4th International Conference on Energy Sustainability. ASME 2010 4th International Conference on Energy Sustainability, Volume 1. Phoenix, Arizona, USA. May 17–22, 2010: 515-22. ASME. https://doi.org/10.1115/ES2010-90218.

[11] Kang J, Chu S, Lee J, Gyujin K, Kyoungdoug M. Effect of operating parameters on diesel/propane dual fuel premixed compression ignition in a diesel engine. Int J Automot Technol 2018;19(1):27–35. https://doi.org/10.1007/s12239-018-0003-6.

[12] Hydrogen Council, Hydrogen Scaling Up: A sustainable pathway for the global energy transition. Brussels, Belgium, 2017. https://hydrogencouncil.com/ en/hydrogen-insights-2021/.

[13] Boretti A. «A dual fuel ICE diesel-H2 featuring 1,600 bar cryogenic liquid H2 injection,» Int. J Hydrog Energy 2021;46(36):19171–9.

[14] Wang J, Cui W, Liu Q, Xing Z, Asiri A, Sun X. Recent Progress in Cobalt-Based Heterogeneous Catalysts for Electrochemical Water Splitting. Adv Mater 2016;28(2):215–30. https://doi.org/10.1002/adma.201502696.

[15] Capurso T, Stefanizzi M, Torresi M, Camporeale S. Perspective of the role of hydrogen in the 21st century energy transition. Energy Convers Manag 2022;251(114898). https://doi.org/10.1016/j.enconman.2021.114898.

[16] Arregi A, Amutio M, Lopez G, Bilbao J, Olazar M. Evaluation of thermochemical routes for hydrogen production from biomass: A review. Energy Convers Manag 2018;165:696–719. https://doi.org/10.1016/j.enconman.2018.03.089.

[17] Kannah RY, Kavitha S, Karthikeyan Preethi OP, Kumar G, Dai-Viet NVO, Banu JR. Techno-economic assessment of various hydrogen production methods – A review. Bioresour. Technol. 2021;319(124175). https://doi.org/10.1016/j.

[18] Aziz M, Darmawan A, Juangsa FB. Hydrogen production from biomasses and wastes: A technological review. Int J Hydrog Energy 2021;46(68):33756–81. https://doi.org/10.1016/j.ijhydene.2021.07.189.

[19] Dincer I. Green methods for hydrogen production. Int J Hydrog Energy 2012;37(2):1954–71. https://doi.org/10.1016/j.ijhydene.2011.03.173.

[20] The Royal Society, Ammonia: zero-carbon fertiliser, fuel and energy store. London, 2020. https://www.royalsociety.org/green-ammonia.

[21] Kurien C, Mittal M. Review on the production and utilization of green ammonia as an alternate fuel in dual-fuel compression ignition engines. Energy Convers Manage 2022;251(114990). https://doi.org/10.1016/j.enconman.2021.114990.

[22] Valera-Medina A, Amer-Hatem F, Azad AK, Dedoussi IC, de Joannon M, Fernandes RX, et al. Review on Ammonia as a Potential Fuel: From Synthesis to Economics. Energy Fuels 2021;35(9):6964–7029. https://doi.org/10.1021/acs.energyfuels.0c03685.

[23] Fernández L. Global production capacity of ammonia 2018-2030. Statista Research Department, 2021. https://www.statista.com/statistics/1065865/ammonia production-capacity-globally/.

[24] Chehade G, Dincer I. Progress in green ammonia production as potential carbon-free fuel. Fuel 2021;299(120845). https://doi.org/10.1016/j.fuel.2021.120845.

[25] MacFarlane D, Cherepanov P, Choi J, Suryanto B, Hodgetts R, Bakker J, et al. A Roadmap to the Ammonia Economy. Joule 2020;4(6):1186–205. https://doi.org/10.1016/j.joule.2020.04.004.

[26] Papadias DD, Peng J-K, Ahluwalia RK. Hydrogen carriers: Production, transmission, decomposition, and storage. Int J Hydrog Energy 2021;46(47):24169–89. https://doi.org/10.1016/j.ijhydene.2021.05.002.

[27] Brynolf S, Taljegard M, Grahn M, Hansson J. Electrofuels for the transport sector: A review of production costs. Renew Sustain Energy Rev 2018;81(2):1887–905. https://doi.org/10.1016/j.rser.2017.05.288.

[28] Bolt A, Dincer I, Agelin-Chaab M. A critical review of synthetic natural gas production techniques and technologies. J Nat Gas Sci Eng 2020;84(103670). https://doi.org/10.1016/j.jngse.2020.103670.

[29] Rasi S, Läntelä J, Rintala J. Trace compounds affecting biogas energy utilisation -A review. Energy Convers Manag 2011;52(12):3369–75. https://doi.org/10.1016/j.enconman.2011.07.005.

[30] Van Den Broek M, Berghout N, Rubin E. The potential of renewables versus natural gas with CO2 capture and storage for power generation under CO2 constraints. Renew Sustain Energy Rev 2015;45:1296–322. https://doi.org/10.1016/j.rser.2015.04.089.

[31] IGU and UN ECE, Joint Report, Natural Gas for Vehicles (NGV). de The 25th World Gas Conference “Gas: Sustaining Future Global Growth”, Kuala Lumpur, Malaysia, 2012.

[32] McKinsey’s global Oil & Gas Practice, Global Gas and LNG Market Outlook to 2035, 2021. https://www.mckinsey.com/industries/oil-and-gas/our-insights/global-gas-outlook-to-2050.

[33] Hernández J, Barba J, Cova-Bonillo A. Autoignition of diesel-like fuels under dual operation with H2. Adv Mech Eng 2019;11(6):1–8. https://doi.org/10.1177/1687814019856781.

[34] Dimitriou P, Kumar M, Tsujimura T, Suzuki P. Combustion and emission characteristics of a hydrogen-diesel dual-fuel engine. Int J Hydrog Energy 2018;43(29):13605–17. https://doi.org/10.1016/j.ijhydene.2018.05.062.

[35] Tsolakis A, Hernández J, Megaritis A, Crampton M. Dual fuel diesel engine operation using H2. Effect on particulate emissions. Energy Fuels 2005;19(2):418–25. https://doi.org/10.1021/ef0400520.

[36] Chintala V, Subramanian K. A comprehensive review on utilization of hydrogen in a compression ignition engine under dual fuel mode. Renew Sustain Energy Rev 2017;70:472–91. https://doi.org/10.1016/j.rser.2016.11.247.

[37] Feng Y, Zhu J, Mao Y, Raza M, Qian Y, Yu V, et al. Low-temperature auto-ignition characteristics of NH3/diesel binary fuel: Ignition delay time measurement and kinetic analysis. Fuel 2020;281(118761). https://doi.org/10.1016/j.fuel.2020.118761.

[38] Reiter A, Kong S. Combustion and emissions characteristics of compression-ignition engine using dual ammonia-diesel fuel. Fuel 2011;90(1):87–97. https://doi.org/10.1016/j.fuel.2010.07.055.

[39] Boretti A. Novel dual fuel diesel-ammonia combustion system in advanced TDI engines. Int J Hydrog Energy 2017;42(10):7071–6. https://doi.org/10.1016/j.ijhydene.2016.11.208.

[40] Sahoo B, Sahoo N, Saha U. Effect of engine parameters and type of gaseous fuel on the performance of dual-fuel gas diesel engines-A critical review. Renew Sustain Energy Rev 2009;13(6–7):1151–84. https://doi.org/10.1016/j.rser.2008.08.003.

[41] Hernández J, Lapuerta M, Barba J. Separate effect of H2, CH4 and CO on diesel engine performance and emissions under partial diesel fuel replacement. Fuel 2016;165:173–84. https://doi.org/10.1016/j.fuel.2015.10.054.

[42] Mancaruso E, Todino M, Vaglieco B. Study on dual fuel combustion in an optical research engine by infrared diagnostics varying methane quantity and engine speed. Appl Therm Eng 2020;178(115623). https://doi.org/10.1016/j.applthermaleng.2020.115623.

[43] American Society for Testing and Materials, ASTM D7668 -Standard Test Method for Determination of Derived Cetane Number (DCN) of Diesel Fuel Oils—Ignition Delay and Combustion Delay Using a Constant Volume Combustion Chamber Method. West Conshohocken, USA, 2014. https://www.astm.org/d7668-14.html.

[44] Linstrom P, NIST Chemistry WebBook. NIST Standard Reference Database Number 69. NIST Office of Data and Informatics, 2021. https://webbook.nist.gov/chemistry/.

[45] Lapuerta M, Hernández JJ, Fernández-Rodríguez D, Cova-Bonillo A. Autoignition of blends of n-butanol and ethanol with diesel or biodiesel fuels in a constant-volume combustion chamber. Energy 2017;118:613–21.

[46] Lapuerta M, Sanz-Argent J, Raine R. Heat release determination in a constant volume combustion chamber from the instantaneous cylinder pressure. Appl Therm Eng 2014;63(2):520–7. https://doi.org/10.1016/j.applthermaleng.2013.11.044.

[47] Lapuerta M, Sanz-Argent J, Raine R. Ignition characteristics of diesel fuel in a constant volume bomb under diesel-like conditions. Effect of the operation parameters. Energy. Fuel 2014;28:5445–54. https://doi.org/10.1021/ef500535j.

[48] Ahmad Z, Kaario O, Qiang C, Vuorinen V, Larmi M. A parametric investigation of diesel/methane dual-fuel combustion progression/stages in a heavy-duty optical engine. Appl Energy 2019;251(113191). https://doi.org/10.1016/j.apenergy.2019.04.187.

[49] Rochussen J, Yeo J, Kirchen P, Effect of Fueling Control Parameters on Combustion and Emissions Characteristics of Diesel-Ignited Methane Dual-Fuel Combustion, SAE Technical Paper 2016-01-0792, 2016. https://doi.org/10.4271/2016-01-0792.

[50] Nguyen D-K, Szybist J, Sileghem L, Verhelst S. Effects of molar expansion ratio of fuels on engine efficiency. Fuel 2020;263(116743). https://doi.org/10.1016/j.fuel.2019.116743.

[51] Ansys, Chemkin-Pro: Chemistry Simulation Software. Version 2021 R2, https://www.ansys.com/products/fluids/ansys-chemkin-pro; 2021 [accessed 13 July 2003].

[52] Luecke J, Rahimi M, Zigler B, Grout R. Experimental and numerical investigation of the Advanced Fuel Ignition Delay Analyzer (AFIDA) constant-volume combustion chamber as a research platform for fuel chemical kinetic mechanism validation. Fuel 2020;265(116929). https://doi.org/10.1016/j.fuel.2019.116929.

[53] Zhu J, Wang S, Raza M, Feng Y, Li J, Mao Y, et al. Autoignition behavior of methanol/diesel mixtures: experiments and kinetic modeling. Combust Flame 2021;228:1–12. https://doi.org/10.1016/j.combustflame. 2021.01.026.

[54] Qian Y, Yu L, Li Z, Zhang Y, Xu L, Zhou Q, et al. A new methodology for diesel surrogate fuel formulation: Bridging fuel fundamental properties and real engine combustion characteristics. Energy 2018;148:424–47. https://doi.org/10.1016/j.energy.2018.01.181.

[55] Ranzi E, Frassoldati A, Stagni A, Pelucchi M, Cuoci A, Faravelli T. Reduced kinetic schemes of complex reaction systems: Fossil and biomass-derived transportation fuels. Int J Chem Kinet 2014;46(9):512–42. https://doi.org/10.1002/kin.20867.

[56] Stagni A, Cavallotti C, Arunthanayothin S, Song Y, Herbinet O, Battin-Leclerc F, et al. An experimental, theoretical and kinetic-modeling study of the gas-phase oxidation of ammonia. React Chem Eng 2020;5:696–711. https://doi.org/10.1039/C9RE00429G.

[57] Klotz S, Brezinsky K, Glassman I. Modeling the combustion of toluene-butane blends. Proc Combust Inst 1998;27(1):337–44. https://doi.org/10.1016/S0082-0784(98)80421-9.

[58] Hartness S, Rotavera B. Dependence of biofuel ignition chemistry on OH-initiated branching fractions. Front Mech Eng 2021;7(718598). https://doi.org/10.3389/fmech.2021.718598.

[59] Pollard R, Hydrocarbons. In: Bamford CH, Tipper CFH, editors. Comprehensive Chemical Kinetics, Elsevier, 1977, p 249-367.

[60] Curran H, Gaffuri P, Pitz W, Westbrook C. A comprehensive modeling study of n-heptane oxidation. Combust Flame 1998;114(1–2):149–77. https://doi.org/10.1016/S0010-2180(97)00282-4.

[61] Zádor J, Taatjes C, Fernandes R. Kinetics of elementary reactions in low-temperature autoignition chemistry. Prog Energy Combust Sci 2011;37(4):371–421. https://doi.org/10.1016/j.pecs.2010.06.006.
[62] Zhu J, Li J, Wang S, Raza M, Qian Y, Feng Y, et al. Ignition delay time measurements and kinetic modeling of methane/diesel mixtures at elevated pressures. Combust Flame 2021;229(111390). https://doi.org/10.1016/j.combustflame.2021.02.036.
[63] Liu F, Liu Z, Sang Z, He X, Liu F, Liu C, et al. Kinetic study of the effects of hydrogen blending to toluene reference fuel (TRF)/air mixtures on laminar burning velocity and flame structure. Fuel 2020;274(117850). https://doi.org/10.1016/j.fuel.2020.117850.
[64] Rezgui Y. A sequential CFD-chemistry investigation of the chemical and dilution effects of hydrogen addition on the combustion of PRF-85 in an HCCI engine. Fuel 2021;292(120299). https://doi.org/10.1016/j.fuel.2021.120299.
[65] Henein N, Bolt J. Correlation of Air Charge Temperature and Ignition Delay for several fuels in a diesel engine. SAE Technical Paper 690252, 1969, https://doi.org/10.4271/690252.
[66] Hernández J, Lapuerta M, Cova-Bonillo A. A novel group-based correlation for the ignition delay time of paraffinic-type fuels. Combust Sci Technol 2019;194(1):80–92. https://doi.org/10.1080/00102202.2019.1678378.
[67] Assanis D, Filipi Z, Fiveland S, Syrimis M. A predictive ignition delay correlation under steady-state and transient operation of a direct injection diesel engine. J Eng Gas Turbines Power 2003;125(2):450–7. https://doi.org/10.1115/1.1563238.